Journal of
Materials Chemistry C

PAPER

View Article Online
View Journal | View Issue

Check for updates

Cite this: *J. Mater. Chem. C*, 2024, **12**, 17305

Received 29th July 2024,
Accepted 5th September 2024

DOI: 10.1039/d4tc03243h

rsc.li/materials-c

Scalable decoration of Au nanoparticles on Al nanoconcavity arrays for highly enhanced SERS detection†

Gohar Ijaz Dar, Elisabet Xifre-Perez and Lluis F. Marsal *

Highly sensitive Raman signal enhancement of target molecules is achieved by developing effective surface-enhanced Raman spectroscopy (SERS) sensing platforms created by a unique combination of plasmonic gold nanofractals and highly ordered nanostructured aluminum arrays. Under efficient laser illumination, the SERS-active substrates formed by Al nanoconcavities of less than 100 nm, each decorated with a single Au nanoparticle, trigger localised surface plasmon resonance. 4-Mercaptopyridine (4-Mpy) successfully interferes on the surface of Au nanofractals, proving the method's utility. As a result, the SERS signal from the 4-MPy adsorbed on Au nanostructures is long-range electromagnetically amplified. The designed and developed substrate brings about a high enhancement factor (EF), over 10^7 increase in intensity when approaching 4-Mpy adsorbed on Au nanostructures. A considerable increase in the SERS signal is found when the excitation origin is determined to be vibrant with the charge transfer (CT) state formed at the interface of the Al nanoconcavities and organic molecules. This approach, which does not need nanopatterning, provides an alternative strategy for conducting SERS investigations on molecules with remarkably weak Raman signals.

1. Introduction and background

In the past couple of years, scientific research has been intensely directed towards the development of tools in the fields of environmental pollution and food safety, concretely focusing on the detection of biological and chemical threats like pathogenic bacteria, their clinical diagnosis, and treatments. Thereupon, developing a dependable and cost-effective tool for the rapid and efficient detection of pathogenic molecules, which enables reproducible and selective fingerprint signatures, is highly demanded.[1] A fast and flexible detection approach, surface-enhanced Raman spectroscopy (SERS), provides unique fingerprint information on analyte molecules and may detect them at the trace level. Because of the electromagnetic mechanism that forms hotspots in the interparticle gaps through localised surface plasmon resonance (LSPR), noble metals are extensively desired as SERS active materials. This is because they strongly boost the Raman signal strength.[2] Developing SERS substrates with substantial hotspots, large surface area, high reproducibility, and uniformity is essential for developing SERS applications.[3] Plasmonic "hot spots" are regions of intensely increased electromagnetic fields that develop once noble metal nanoparticles are exposed to visible light; these spots serve as triggers for SERS activity. Various techniques exist to synthesise the SERS substrates for highly sensitive and reproducible performance.

The immense enhancement of the local surface of the dense Raman signals of the substrates makes them more interesting and attractive. Nevertheless, several obstacles interfere with the practical application of nanoparticulate systems in SERS. These include technical issues such as aggregation, heterogeneous size and shape distributions, and regulatory constraints related to environmental and health concerns, such as uncertainty regarding nanomaterials' eventual use and contaminants, which reduces the enhancement factor (EF).[4] To overcome these problems, 2D plasmonic single- and super-lattices can be used to transfer systems of nanoparticles based on noble metals onto substrates that are both adaptable and mechanically strong. There have been reports on extremely strong resonance bands in the visible spectrum produced by single and super-lattice LSPR modes, which can be tuned across a wide frequency range by adjusting the geometric properties of the lattice unit. Building noble metal-based single- and super-lattices with precisely regulated nanometric features is possible using direct writing techniques like electron beam lithography and focused ion beam lithography. Despite this, these methods are expensive

---

Departament d'Enginyeria Electrònica, Elèctrica i Automàtica, Universitat Rovira i Virgili, Avinguda Països Catalans 26, Tarragona 43007, Spain. E-mail: lluis.marsal@urv.cat

† Electronic supplementary information (ESI) available. See DOI: **https://doi.org/10.1039/d4tc03243h**

(about \$2 million in capital expenditure), non-scalable (limited to mm^2), and time-consuming (around 12 to 24 hours).[5,6] These reported techniques are much more expensive, have low outcomes, and are less appropriate for various structures and materials, such as 3D nanostructures, that exhibit high SERS sensitivity.

The magneton sputtering mechanism can be defined as the physical vapour deposition technique employed to deposit thin metal films onto various substrates for scientific and commercial intentions.[7] This cost-effective method has shown that 2D nanoplasmonic lattices can improve electromagnetic field performances for SERS applications by combining hybrid plasmonic and photonic resonances in structurally optimised ways. This is one of the simplest strategies to overlook the growth control as well as the morphology of deposited metals and is dependent on the use of porous mixture templates such as porous silicon, alumina, TiO_2, and various additional materials, in which the morphology, arrangement, and dimensions of the pores decide the localization of the organized noble metal nanostructures.[8,9] Optimal homogeneity over nano and macroscopic areas for functioning in the visible-NIR spectral range is still a basic and applied topic in nanofabrication, considering recent advances. An important step towards comprehending and using complicated hybrid plasmonic resonance modes for SERS is the development of model metal-based nanoparticle lattices integrated into functional substrates with appropriate shapes and features. In addition to various metals, gold (Au) has attracted the promising attention of researchers for its high stability and optical and biocompatible properties.[10,11] Furthermore, tuning the shape and size of Au nanostructures can lead to a new window with unique properties that differ distinctly from those reported in individual nanoparticles or bulk metal solids. Among various existing templates, porous anodic alumina oxide synthesized using an electrochemical approach was referred to as the best template to engineer the deposited metallic nanostructure owing to its high density and spatial resolution.[12,13]

In this work, we develop Al nanoconcavity array templates with Au nanoparticles assembled *via* sputtering and thermal treatment. The Al nanoconcavity template, obtained by electrochemical anodization, has high morphological flexibility, allowing the adjustment of the concavity size from $\approx$40 to 450 nm depending on the electrolyte used. Magnetron sputtering onto Al nanoconcavity arrays forms Au nanostructures with large size and distribution uniformity owing to its high spatial resolution. Here, formed Au nanoparticles are well accumulated into the patterned Al nanoconcavities with one particle per concavity. The resultant patterned Au nanoparticle accumulation onto the Al nanoarrays have a high spatial resolution with tuneable plasmonic bands that are visible in the NIR region.

2. Experimental section

2.1. Materials and chemicals

Highly pure (99.99%) aluminium sheets (Al) with a thickness of 0.3 mm had been purchased from Goodfellow Cambridge Ltd, in the United Kingdom. Oxalic acid ($H_2C_2O_4$), ethanol (C_2H_5OH, EtOH), acetone ($(CH_3)_2CO$), perchloric acid ($HClO_4$), chromic acid (H_2CrO_4), hydrochloric acid (HCl), and 4-mercaptopyridine (96% AR) were supplied by Sigma Aldrich. Ultra-pure water was used in the preparation of aqueous solutions.

2.2. Fabrication of the Al nanoconcavities

Al foils were carefully cut into 2 × 2 cm^2 templates to refrain from bending and soaked with acetone, water, and ethanol to release any signs of impurities and grease. Immediately, the samples were electropolished on one side with a mixture of perchloric acid–ethanol solution 4 : 1 v/v at 20 °C for 6 minutes, modifying the stirrer direction every 60 s. Electropolishing was carried out using a twin-electrode setup with an applied voltage of 20 V. After electropolishing, they were cleaned with water and ethanol and dried with compressed air. Then, the samples were ready to be employed for the anodization process.

Various studies have been reported in the literature regarding the anodization process for oxalic acid.[14–18] The oxalic acid two-step anodization is initiated on Al sheets by selecting the analyte temperature at 5 °C and applying a voltage of 40 V for 24 h. Subsequently, to remove the disordered pattern surface formed on the Al template after first anodization, the substrates were immersed in the chemical etching solution (chromic acid (1.8%) and phosphoric acid (6 wt%)) and vigorously stirred for 2 h at 75 °C. After cleaning with water, the next anodization step was acquired under the same conditions for 3 h,[19,20] forming a porous layer of anodic aluminium oxide (AAO) with a hexagonally and highly ordered pore distribution on the Al template. When this AAO layer is removed with the previously used chemical etching solution at 70 °C for 2 h, the resultant Al substrate is patterned with a highly uniform and ordered distribution of nanoconcavities. The synthesis process of aluminium concavities enriched with Au fractals is depicted in steps in Fig. 1.

2.3. Au nanoparticle formation on the Al nanoconcavity templates

The fabricated Al templates with hexagonally arranged nanoconcavities are the base for the final SERS substrates. For this goal, Au nanoparticles perfectly positioned inside the nanoconcavities are formed following a procedure initiated by sputtering Au thin films on the Al templates. Primarily, the sputtering process was executed *via* magnetron sputtering (BESTEC, magnetron sputtering system) composed of the Au target (99.99%) with defined conditions, the Ar flow rate was 20 sccm, the pressure was 3 mTorr, and the Rf power was 30 W. We experienced various sputtering time intervals (20, 60, 108, and 200 s) to prepare the effective SERS substrates. Subsequently, the Au-sputtered Al templates were thermally treated at variable temperatures and time intervals to examine the resultant morphology of the Au fractals. The resultant formation of the Au nanoparticles is strongly dependent on the thermal temperature and time and can be altered by changing these parameters.

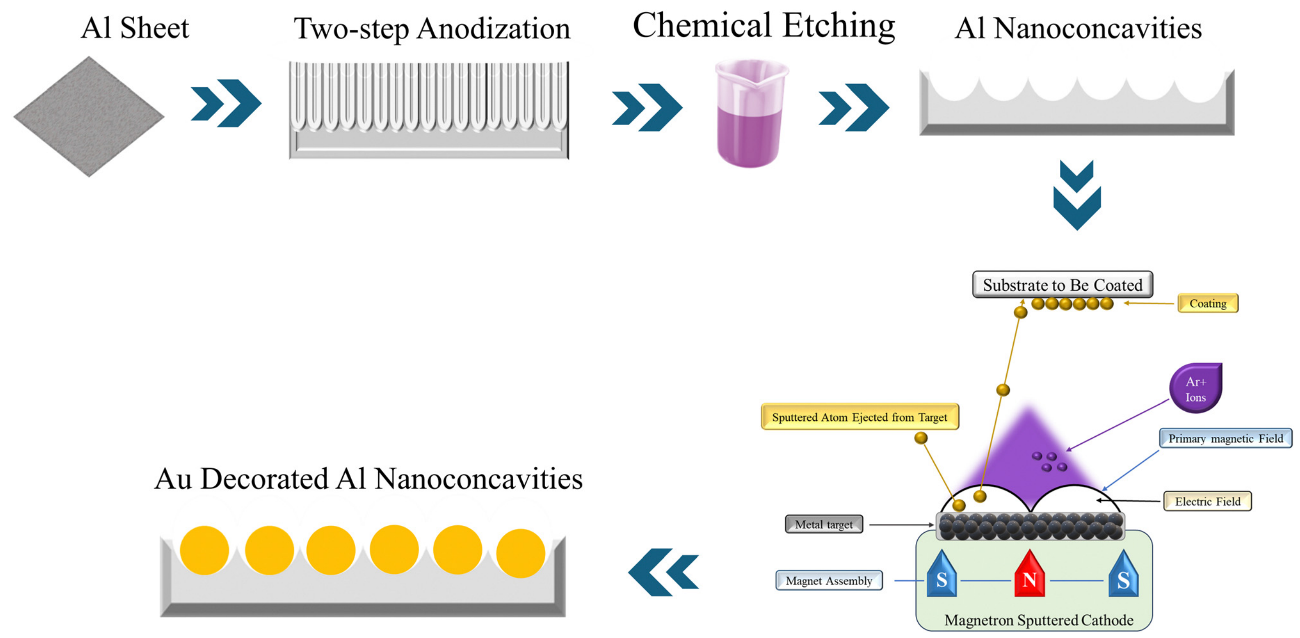

Fig. 1 Experimental steps for synthesis of Al nanoconcavity arrays enriched with Au fractals.

2.4. SERS measurements

A confocal Raman micro spectrometer (Renishaw inVia Raman Microscope) was used to record the SERS spectra. The instrument was equipped with a 785 nm excitation laser, a 1200 lines per mm grating, and a 50X LWD objective lens. During the measurement process, the laser intensity was set at 10 milliwatts, the laser spot diameter was approximately 1 micrometre, and the exposure period for each substrate was 10 s.

2.5. Substrate preparation for SERS activity

The SERS spectra were recorded for the prepared substrates with Au sputtered for 20, 60, 108, and 200 s and thermally treated at different temperatures (350 °C for 30 min, 400 °C for 30 min, and 400 °C for 120 min). 4-Mercaptopyridine (4-Mpy) was selected as the target analyte to investigate the SERS activity of the prepared substrates. 4-Mpy is also generally represented as sodium pyrithione and is a pyridine derivative used in experiments with an association of thiosulfate to regulate the alliinase activity.[21] 4-MPY concentrations were used for SERS detection: a lower concentration of 10^{-7} M and a higher concentration of 0.1 M. The 0.1 M 4-Mpy aqueous solution was used as the control, whereas the 10^{-7} M concentration of 4-Mpy was employed on Al nanoconcavity substrates gold-sputtered and annealed. Both 4-Mpy aqueous solutions were dropped off on the Al nanoconcavity templates and waited to dry entirely.

3. Results and discussion

The ability to precisely modify the shape and dimensions of the nanoparticles on the template is still topical. It depends on various factors in our process, such as the template's size and morphology, the deposited metal's sputtering time, and the l annealing temperature.

Thermal annealing treatment includes either coalescence and migration of Au nanoparticles or Au atom migration (Ostwald ripening).[22] The coalescence process exists when two nanostructures become one considerably big particle. Throughout particle conjugation, nanoparticles could relocate to the surface of the substrate and coalesce if the movement bears the reduction in primary system energy. In contrast, Ostwald ripening happens when the atoms are removed from one nanostructure and delivered to another *via* surface diffusion or evaporation. In this scenario, a reduction in surface energy is responsible for mass transport without any particle contact between them. So, both nanostructures trade their atoms, resulting in tiny nanoparticles by atom depletion, while larger ones become larger through atom accumulation. The Ostwald ripening phenomenon is the basic strategy of thermal annealing for well-separated metal nanoparticles sustained on the surface, while coalescence could refer to clusters with high-density.[23]

As described earlier, the Au film was deposited *via* the sputtering process. The enhanced motion of Au atoms during the sputtering process results in a smooth Au layer on the exposed surface of the substrate. Here, we employed the reagent-free physical evaporation deposition (PVD) technique through a sputtering mechanism to deposit Au at various times (20, 60, 108, and 200 s). When the deposited Au film is treated *via* thermal annealing, it initiates interaction with the landscape beneath the Al nanoconcavity arrays. Multiple pre-existing cracks in the uncontrolled Au film acted as nuclei during thermal annealing treatment. As the sputtering time proceeds, they become larger and undergo homogeneous formation of Au nanoparticles at the centre of the Al nanoconcavity with a limited diameter and reduced interparticle distance. These interstitial localities tend to be strong LSPRs having concentrated electromagnetic fields.[24]

In our study, our goal is to utilize the Al nanoconcavity morphology template for SERS activity. In the ideal situation, one particle should be accommodated in a single concavity.[24] The size and formation of the Au nanoparticles depend on the deposited metal film annealing treatment and the corresponding volume of the nanoelemental cell. The theory of surface energy minimization explains the driving force responsible for the synthesis of nanoparticles, as already discussed for similar morphologies by Fan and others.[24] This desired accommodation of the formed Au nanoparticles in a single concavity could be an effective SERS template.[24]

In Fig. 2a–c, the FESEM images reveal the substrates obtained with Au sputtering for 20 s and several annealing temperatures and times: 350 °C for 30 min, 400 °C for 30 min and 400 °C for 120 min. The images show the presence of Au aggregations of a few nanometers in diameter and gaps between them on the surface structure because of the local stress invoked by the Al nanoconcavity array.[25] The substrates obtained with Au deposited for 60 s are observed in Fig. 2d–f for the above-mentioned annealing parameters. The Au nanostructure formation is improved compared to the 20 s Au deposition results: several small Au patches are formed in a single cell. Fig S1 and S2 (ESI†) show the corresponding pictorial and quantitative EDS analyses.

For both sputtering times (20 and 60 s), the resulting nanostructures exhibit an unwanted large interparticle separation, which is not productive in enhancing plasmon coupling. If the interparticle separation becomes too large, interparticle plasmon coupling will not be observed, leading to non-observable

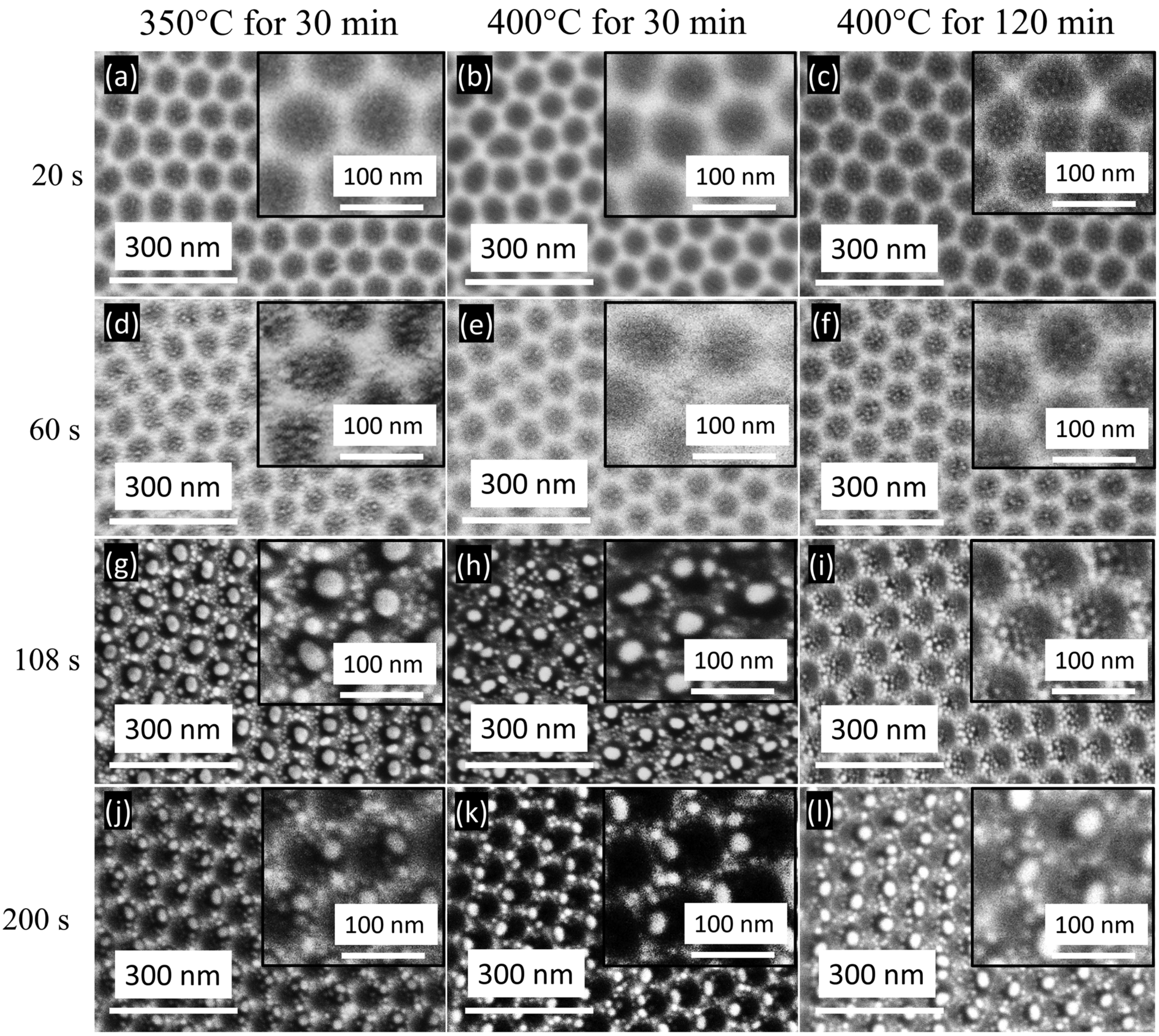

Fig. 2 FESEM images of Au deposited on Al nanocavity substrates for 20 s (a)–(c), 60 s (d)–(f), 108 s (g)–(i) and 200 s (j)–(l) with various thermal annealing treatments and the corresponding magnification (inset).

LSPR refractive index sensitivity.[26] Therefore, we aim to decrease the interparticle distance and increase the Au particle size of the formed nanostructures by tuning the Au deposition time and the annealing treatment parameters.

To achieve this goal, the increment of the deposition time is further studied. When the Au deposition time is increased to 108 s, the annealing procedure dissolves the deposited Au layer. An array of one Au nanoparticle per concavity is obtained, revealing the direct association of Au nanoparticles and concavity positions (Fig. 2g–i). Besides, numerous tiny Au nanoparticles are observed on the surface edges of the nanoconcavities. Also, the nanoconcavity honeycomb-like morphology is still prominent. For 350 °C for 30 min and 400 °C for 30 min annealing, most nanoconcavities have a single nanoparticle inside, suggesting an atomic diffusion process that progressed from microscopic particles to bigger ones.[27] In contrast, for 400 °C for 120 min, this progression is not experienced and several small nanoparticles in each nanoconcavity are observed. The resultant morphology of Au nanoparticles after sputtering for 108 s is completely different from those achieved with the previously studied sputtering times (20 and 60 s), exhibiting larger particles, each one positioned in one nanoconcavity. When the Au sputtered on the Al nanoconcavities undergo thermal annealing, the Au film reacts with the topography of the nanoconcavities. The driving force that is responsible for the formation of ‘one particle per concavity’ can be illustrated by surface energy minimization theory.[28] The Gibbs-Thomson equation is $\Delta\mu = \kappa\gamma\Omega$, where $\Delta\mu$ refers to the local chemical potential, Ω is the atomic volume, γ is the surface energy, and κ represents the local curvature intended for the Au atoms spread away from the protrusion to the concavity to minimize the local curvature and surface energy, leading to a reduction of the local excess chemical potential.

However, for 108 s sputtering, the thermal annealing of 400 °C for 120 min causes the aggregation of the Au nanostructures with numerous tiny nanoparticles at the center of the nanoconcavity, and larger nanoparticles at the edges, having an undesirable interparticle separation between them (Fig. 2i). Indeed, the heat 400 °C for 120 min transferred to this Al substrate leads to the undesirable formation of resultant Au nanostructures. The resultant nanostructures would not yield considerable SERS sensitivity by plasmon coupling, and therefore, the annealing for 120 min at 400 °C would not be favorable for Au deposition of 108 s.

The sputtering time and annealing conditions are vital in forming deposited nanostructures. When the sputtering time increases, the morphology and number of particles vary. The 200 s Au deposition on the Al nanoconcavity substrates has also been analyzed for further investigation for the annealing parameters under study (Fig. 2j–l). For thermal annealing of 350 °C for 30 min (Fig. 2j), the image reveals a nonhomogeneous formation of Au nanostructures that hinders the clear vision of the concave structure. Various nanoparticles are formed in the vicinity of larger particles and merge with others. Interestingly, when the thermal annealing of 400 °C is applied only for 30 min, the results reveal fascinating Au structures formed inside the nanoconcavities as shown in Fig. 2k: every single cell is occupied by one Au nanoparticle, which can be an ideal situation for the deposited metal to achieve the nanoplatforms for various applications related to plasmon resonance.[25] The number of particles and morphology is particularly homogeneous, leading to an interesting substrate for SERS activity. Furthermore, the deposition time thickness and film morphology are required to make the analogous nanostructures with a defined template configuration. The film morphology varies with the selected technique and its applied parameters. Here, magnetron sputtering was chosen with various Au deposited times, yet it brings on the unperturbed film compared to other mechanisms. However, deep studies of the deposition techniques are not our current purpose. The graphical and quantitative EDS analysis for the Au deposited for 20, 60, 108 and 200 s are shown in Fig. S1–S4 in the ESI,† respectively.

3.1. SERS measurements

The phenomenon of vibronic coupling, which involves the interaction of surface plasmon, exciton, charge-transfer, and molecular resonances, has been suggested as the underlying cause for the significant enhancement observed in surface-enhanced Raman scattering (SERS) in both metals and semiconductors. 4-Mpy is utilized as a probe molecule to evaluate the SERS activity of Au-decorated Al nanoconcavity templates. 4-MPy is a typical aromatic thiol molecule composed of a para-position thiol group coupled to an N atom in the pyridine ring. This unique structure enables it to bond to metal surfaces, which has interesting applications in domains such as sensor optics and catalysts.[29–31] Here, we investigate the SERS ability of the Au nanostructure formed onto the Al nanoconcavities with Au deposition times of 20,60, 108, and 200 s and thermally treated at the above-mentioned temperatures and times. We evaluate and compare every prepared sample to evaluate its potential for highly sensitive SERS substrates. A concentration of 10^{-7} M 4-Mpy deposited on each of the evaluated substrates generates SERS signals with numerous 4-Mpy characteristic Raman shifts. The Raman spectroscopy measurement of the control substrate is performed with 0.1 M 4-Mpy in an aqueous solution.

According to the literature, the peak location is mentioned in SERS graphs, along with their assignments modes such as 713, 1007 and 1099 assigned a1 while 1065 and 1213 assigned b2 layout in Fig. 3–6.[32,33] The SERS activity of the substrates fabricated with Au deposition of 20 s for the temperatures and times under consideration is observed in Fig. 3. No significant peaks of 4-Mpy are detected for any template. Only minor signals are observed at 1005 and 1098 cm^{-1} Raman shifts for the sample thermally treated at 400 °C for 120 min. As we noticed on the FESEM image of this substrate (Fig. 2c), the formed Au nanostructures are not well visible nor distributed homogeneously to make hotspots for SERS activity, and the bigger Au nanoparticles of this substrate do not scatter enough light to make the minimum contribution to SERS amplification. Traditional SERS is thought to have a surface EF of approximately 10^3 to 10^6 due to the combined effects of two enhancement processes, each having its own signature size

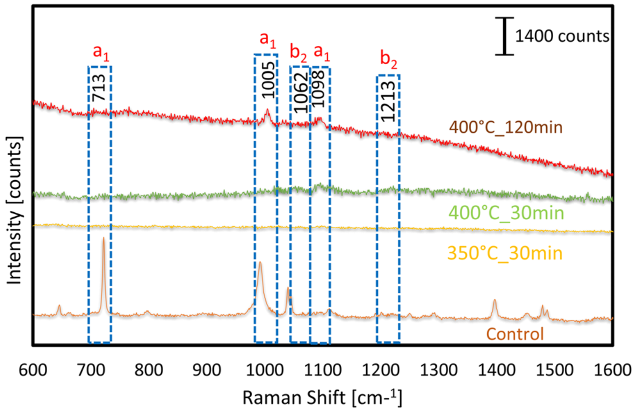

Fig. 3 SERS spectra of 20 s Au-sputtered substrates with thermal annealing at various temperatures and time intervals. The concentration of 4-Mpy for the control substrate is 0.1 M, and that for the rest of the substrates is 10^{-7} M.

scale of surface roughness. It is hypothesized that the large-scale roughness in the 10–100 nm region adds a factor of 10^4 to the overall EF *via* a long-range, classical, electromagnetic enhancement process. This is because the laser-triggered surface plasmon resonances in the nanoscale metal clusters result in a massive rise in the electric field. On the other hand, the CHEM enhancement process is credited with a factor of enhancement of $\sim 10^1$–10^2. It is seen as a short-range phenomenon necessitating an orbital overlap between the surface's topmost layer of atoms and the adsorbate. Each kind of charge transfer related to chemisorption occurs on a different length scale of the surface roughness.[34] The Au–S bond provided a natural attachment route for the 4-MPy molecules to connect to Au. Strong Au–S bonds can be initiated when the sulfhydryl group in 4-MPy binds to the Au sites on the Al substrate. When the sputtering duration and annealing temperature are varied, the resulting Au fractals display varying degrees of symmetry, and the SERS activity varies in order and magnitude according to the size of the fractals and the distances between them. There is a direct correlation between concentration and Raman intensity, and it has been reported that a low concentration cannot be efficiently adsorbed on a substrate.[35] Nevertheless, the low Raman signal was observed at high concentrations because the Au nanoparticles aggregated at those concentrations.[36,37]

The SERS activity for detecting 4-Mpy of substrates with Au deposition of 60 s has also been studied. The corresponding FESEM images (Fig. 2d–f) of these substrates demonstrated that formed Au nanostructures are comparatively better than the ones obtained for 20 s Au deposition. Therefore, the SERS signals are expected to present higher magnification. The SERS measurements (Fig. 4) reveal various prominent peaks at 1006 and 1096 cm^{-1} bands detected with the templates annealed at 350 °C for 30 min and 400 °C for 120 min. These SERS peaks are well matched with the previous literature and present for the control substrate. The band at 1096 cm^{-1} corresponds to X-sensitive modes, which are described as modes that are tightly connected between aromatic and replacement ring modes. Ring breathing modes are allocated to the band at 1006 cm^{-1}, while CH deformation is assigned to the band at 1066 cm^{-1}. All the above bands are equivalent to SERS of 4-Mpy adsorbed on Au nanoparticles, as reported previously.[32,33]

However, the SERS signal for the template prepared with 400 °C for 30 min does not present any prominent peak and cannot be considered for SERS activity. Although some peak bands are observed, the nanostructures do not scatter most of the incident light, probably due to various factors such as the interparticle distance, the absence of hot spots, the size, and the distribution of the nanostructures. The SERS activity for 108 s Au sputtering deposition and subsequent thermal annealing is presented in Fig. 5, Also, for a 4-Mpy concentration of 10^{-7} M, an important improvement in the SERS amplification was observed with Au sputtering. Various Raman peaks are clearly identified for 4-Mpy detection: 713, 1007, 1099, and 1213 cm^{-1} compared to the control. All the prepared samples reveal a notable SERS enhancement. The higher sharpness of

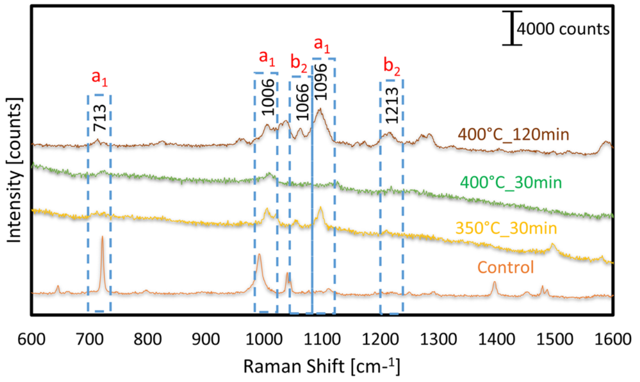

Fig. 4 SERS spectra of 60 s Au-sputtered substrates with thermal annealing at various temperatures and time intervals. The concentration of 4-Mpy for the control substrate is 0.1 M, and that for the rest of the substrates is 10^{-7} M.

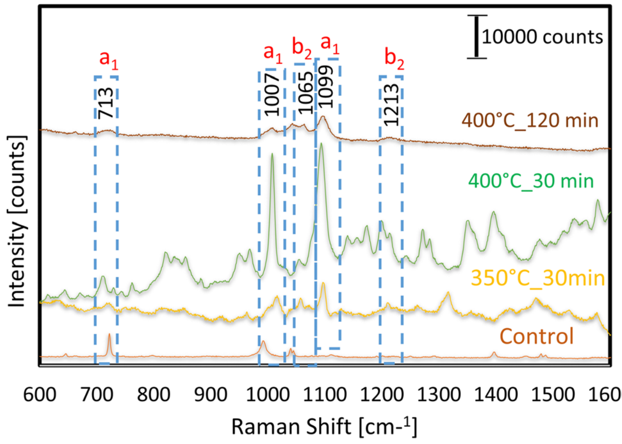

Fig. 5 SERS spectra of 108 s Au-sputtered substrates with thermal annealing at various temperatures and time intervals. The concentration of 4-Mpy for the control substrate is 0.1 M, and that for the rest of the substrates is 10^{-7} M.

signals was observed in the templates annealed at 350 °C and 400 °C for 30 min. Their nanoconcavity layer helped to ensure that even the most tightly packed Au nanostructures dispersed evenly, preventing them from clustering together. Intense amplification of the Raman signal was possible because of the huge surface area of the nanoconcavities and the high density of the formed nanostructures. Specifically, the AuNP-modified substrate significantly boosts the SERS peaks at 1007 and 1099 cm^{-1}.

The enhancement of the SERS response of the 108 s Au deposition substrates in comparison with the ones with 20 and 60 s deposition was expected with the observation of the FESEM images in Fig. 2. For the ideal case, when an Au thin film is thermally annealed on top of an aluminum nanoconcavity template, one nanoparticle is formed for every dimple, with a volume proportional to the area of the dimple and the thickness of the deposited film. The hexagonal protrusions on the template play a primary regulating role here since their uniform sharpness and confinement of nanoparticle development zones make this possible. As observed in Fig. 2g, h and j–l, one well-defined Au nanoparticle of a considerable size is located inside each nanoconcavity. When all other factors and techniques remain constant, we found that the relative intensities of the bands in the spectra of the various templates exhibit striking differences. We are investigating the suitability for the SERS enhancement of the templates fabricated with 200 s Au deposition. As shown in Fig. 6, these templates' most prominent 4-Mpy Raman peaks are positioned at 713, 1007, and 1095 cm^{-1}, respectively. The band at 1095 cm^{-1} corresponds to the so-called X-sensitive modes, which are described as the modes that are closely connected between aromatic and replacement ring modes. The band at 1213 cm^{-1} is designated for N–H stretching and C–H deformation modes, respectively.

For the 200 s sputtering time, all the annealing conditions analysed result in substrates producing SERS amplification. However, this amplification is not as high as the ones obtained with the 108 s sputtering substrates, which were demonstrated to be the most interesting and extremely suitable substrates for SERS detection. The effectiveness of the SERS signal magnification for both the band at 1007 cm^{-1} and the band at 1065 cm^{-1} is attributable to CH deformation. The band at 1007 cm^{-1} is associated with ring breathing modes. However, this amplification is not as high as the ones obtained with the 108 s sputtering substrates, which were demonstrated to be the most interesting and extremely suitable substrates for SERS detection. The effectiveness of the SERS signal magnification for the Au-decorated Al nanoconcavity substrates was studied further. A typical method to objectively determine SERS proficiency is calculating the enhancement factor (EF). We have followed the most standard and accurate method[38] for its determination, as expressed in eqn (1):

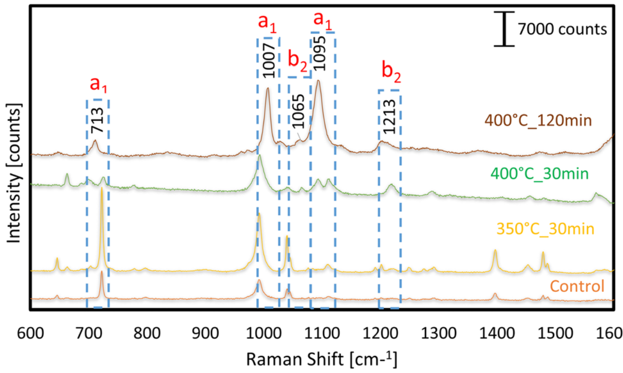

Fig. 6 SERS spectra of 200 s Au-sputtered substrates with thermal annealing at various temperatures and time intervals. The concentration of 4-Mpy for the control substrate is 0.1 M, and that for the rest of the substrates is 10^{-7} M.

$$EF = (I_{surf}/N_{surf})(I_{bulk}/N_{bulk}) \quad (1)$$

where the intensities of the vibrational modes in the SERS and Raman spectra are denoted as I_{surf} and I_{bulk}, respectively, N_{bulk} is the total number of molecules subjected to Raman spectrum analysis, and the number of molecules subjected to SERS probes is denoted by N_{surf} (see the ESI† for more details). We calculate and evaluate the EF for all the fabricated substrates to evaluate the most suitable fabrication parameters of the Au nanoparticle Al nanoconcavity platforms. Table 1 indicates the EF values of the significant peaks identified with 4-Mpy detection for the developed templates where SERS signals were detected. From these results, we can distinguish the fabricated substrate for SERS detection with the highest EF, which is that obtained with Au sputtering for 108 s and thermal annealing of 400 °C for 30 min, with an EF > 10^7 for both bands: 3.4 × 10^7 for 1009 cm^{-1} and 1.6 × 10^7 for 1097 cm^{-1}. This highest EF substrate presents the largest single Au nanoparticles inside nanoconcavities of all the fabricated SERS substrates (see Fig. 2h). According to Xia *et al.*,[39] the larger particles tend to scatter light more efficiently than smaller ones. The superior scattering efficiency of the Au nanoparticles for this substrate could be the main reason for its highest EF.[39] The important contribution of the nanoparticles size to the EF is also supported by the nanoparticle size of the 2nd and 3rd best EF substrates (200 s Au sputtering and thermal annealing of 400 °C for 120 min and 108 s Au sputtering and thermal annealing of

Table 1 EF calculations for 4-Mpy detection against all the prepared substrates

Sputtering time	Thermal annealing	EF for 1009 cm^{-1}	EF for 1097 cm^{-1}
20 s	350 °C_30 min	1.9 × 10^5	1.0 × 10^5
	400 °C_30 min	3.6 × 10^5	1.9 × 10^5
	400 °C_120 min	1.1 × 10^6	2.8 × 10^5
60 s	350 °C_30 min	1.7 × 10^6	1.8 × 10^6
	400 °C_30 min	1.2 × 10^6	4.5 × 10^5
	400 °C_120 min	1.3 × 10^6	1.5 × 10^6
108 s	350 °C_30 min	6.9 × 10^6	4.4 × 10^6
	400 °C_30 min	**3.4 × 10^7**	**1.6 × 10^7**
	400 °C_120 min	1.3 × 10^6	2.9 × 10^6
200 s	350 °C_30 min	3.3 × 10^6	5.2 × 10^5
	400 °C_30 min	2.7 × 10^6	1.2 × 10^6
	400 °C_120 min	**1.5 × 10^7**	7.9 × 10^6

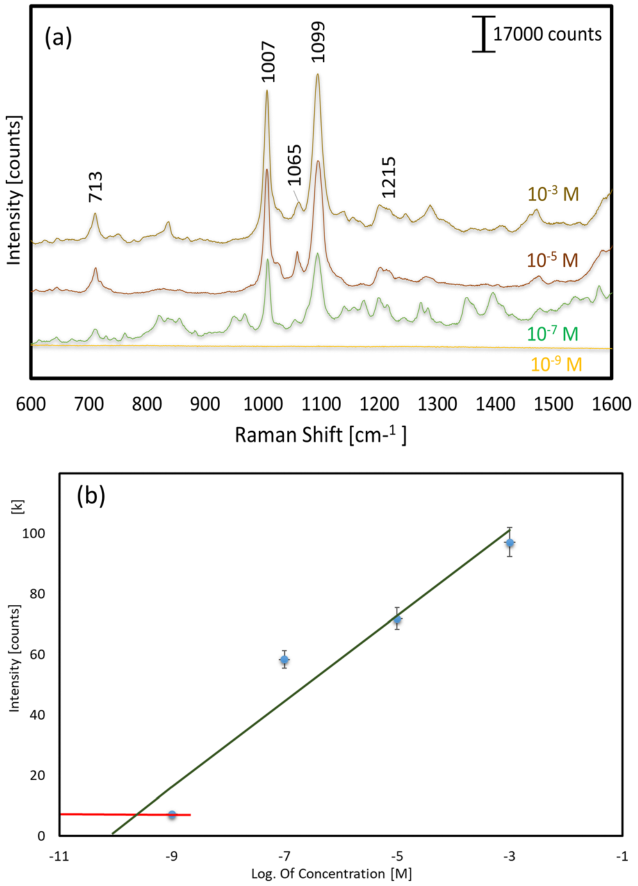

Fig. 7 SERS spectra of 108 s Au sputtered substrates with thermal annealing at 400 °C for 30 min for various 4-Mpy concentrations (a), and the corresponding linear fitting curve for various concentrations to identify the quantification region (red line corresponds to region of insufficient concentration) (b).

350 °C for 30 min, respectively) (Table 1) that, in turn, are the substrates with the next highest nanoparticle size. In addition to the main contribution of the nanoparticle size, the enhancement of the SERS signal can also be promoted by the consequent reduction of the interparticle distance and the additional presence of small nanoparticles at the nanoconcavity edges that form several hotspots.[40,41]

SERS substrates with similar EFs are reported in recent and exciting findings in SERS research, but are obtained with completely different approaches. Dzhagan *et al.* reported an EF of $\sim 10^8$ in the detection of rhodamine 6G with self-organization of Ag nanoparticles on silica spheres.[40] Fu *et al.* reported Ag_2S substrates for SERS to detect 4-Mpy with an EF of 10^3.[42] Further SERS substrates were also reported based on the direct growth of GNPs into porous anodic alumina on conductive glass, which had an EF of 10^6, while the molybdenum disulfide monolayer-based substrate revealed an EF of 10^5.[43,44] By directly comparing all the SERS peaks and the corresponding EFs reported in the references with matching peaks for the detection of 4-Mpy, it can be observed that an EF of 3.4×10^7 presented by our platform with Au sputtering for 108 s and thermal annealing of 400 °C for 30 min provides the highest SERS magnification of 4-MPy.

The substrates developed in this work have fascinating structures for surface-enhanced Raman spectroscopy (SERS) activity. They are obtained with completely controlled and reproducible anodization conditions. This characteristic leads to important homogeneity and reproducibility of the location, size and shape of nanoparticles, that, in turn, results in very repeatable SERS signals all over the substrate. Signal improvement can be unpredictable in many alternative SERS substrates reported elsewhere due to unevenly distributed hotspots and the randomness of the metal nanoparticles position and size, and where nanoparticles can cluster randomly.[45,46]

To further investigate the SERS performance and suitability of these substrates, for our most promising substrate (108 s sputtering and 400 °C-30 min annealing), we evaluated its SERS response to various concentrations of 4-Mpy (Fig. 7a). This analysis was conducted using a Raman shift value of 1097 cm^{-1}. The curve serves to identify the region suitable for quantification purposes. The red line denotes the region of the insufficient concentration, rendering quantification unattainable (Fig. 7b). The study's findings indicated that this substrate exhibited significant outcomes at concentrations of $\geq 10^{-7}$ M of 4-Mpy. No signal was detected for the detection of 4-Mpy at a concentration of 10^{-9} M or below. Although other works report the detection of lower concentrations of 4-MPy,[45,47] it would be possible to increase the limit of detection of our SERS substrates by scaling the nanoparticle ordered distribution (smaller interparticle distances could be easily obtained by simply using different anodization electrolytes, *e.g.* sulphuric acid). The ease of fabrication of the presented SERS substrates makes them also suitable for applications requiring reproducible and cost-effective fabrication processes.

4. Conclusions

In conclusion, this study provides a robust method for assembling Au nanoparticles in high-density nanoarrays with superior spatial resolution by using Al nanoconcavity array templates fabricated electrochemically and a simple magnetron sputtering process. A series of ordered Au nanoarrays with 'one particle per concavity' are successfully fabricated by carefully controlling the geometry of the Al nanoconcavity array template, the Au sputtering time, and the thermal treatment parameters. Based on our findings, not all Au-sputtered nanoconcavity substrates are suitable for high-sensitivity SERS activity. The best evaluated conditions for fabricating high EF SERS substrates were found to be 108 s Au sputtering time and a thermal annealing treatment of 400 °C for 30 min. With an EF of 3.4×10^7 at 1009 cm^{-1}, the prepared AuNP decorated Al nanoconcavity templates are the most sensitive SERS substrates reported in the literature to our knowledge for detecting 4-Mpy. These novel SERS substrates have broad utility for detecting many molecules, including those for which a highly amplified SERS signal is crucial.

Author contributions

G. I. D. and Dr E. X. P. conducted the experiments. Professor L.F.M. came up with the idea and planned the experiments for this study. Each contributor assisted in a panel discussion and analysis of the results. All contributors have made significant contributions to the writing of the manuscript. Each author has read and approved this version of the manuscript.

Data availability

Data for this article are available at ''Replication Data for: Scalable Decoration of Au Nanoparticles onto Al Nanoconcavities Arrays for Highly Enhanced SERS Detection'' at https://doi.org/10.34810/data1519.

Conflicts of interest

The authors have no conflicts to disclose.

Acknowledgements

This project has received funding from the European Union's Horizon 2020 research and innovation program under the Marie Skłodowska-Curie grant agreement No. 945413 and from the Universitat Rovira i Virgili (URV). This work was supported by the Spanish Ministerio de Ciencia e Innovación (MICINN/FEDER) PDI2021-128342OB-I00, by the Agency for Management of University and Research Grants (AGAUR) ref. 2021-SGR-00739, COST Action 20126-NETPORE and by the Catalan Institution for Research and Advanced Studies (ICREA) under the ICREA Academia Award.

References

1 G. Luo, J. Zhang, Y. Sun, Y. Wang, H. Wang, B. Cheng, Q. Shu and X. Fang, *Nano-Micro Lett.*, 2021, **13**, 1–64.
2 D. Grasseschi and H. E. Toma, *Coord. Chem. Rev.*, 2017, **333**, 108–131.
3 Z. Starowicz, R. Wojnarowska-Nowak, P. Ozga and E. Sheregii, *Colloid Polym. Sci.*, 2018, **296**, 1029–1037.
4 M. Rycenga, P. H. Camargo, W. Li, C. H. Moran and Y. Xia, *J. Phys. Chem. Lett.*, 2010, **1**, 696–703.
5 F. Tian, F. Bonnier, A. Casey, A. E. Shanahan and H. J. Byrne, *Anal. Methods*, 2014, **6**, 9116–9123.
6 L. Ouyang, W. Ren, L. Zhu and J. Irudayaraj, *Rev. Anal. Chem.*, 2017, **36**, 20160027.
7 F. Shi, *Magnetron Sputtering*, IntechOpen, 2018.
8 C. Eckstein, E. Xifre-Perez, M. Porta-i-Batalla, J. Ferre-Borrull and L. F. Marsal, *Langmuir*, 2016, **32**, 10467–10472.
9 S. Khan and E. Stamate, *Nanomaterials*, 2022, **12**, 1539.
10 H. Zhang, X. Ma, Y. Liu, N. Duan, S. Wu, Z. Wang and B. Xu, *Biosens. Bioelectron.*, 2015, **74**, 872–877.
11 E. Xifre-Perez, J. Ferre-Borull, J. Pallares and L. F. Marsal, *Open Mater. Sci.*, 2015, **2**, 13–32.
12 J. Ferré-Borrull, E. Xifré-Pérez, J. Pallarès and L. F. Marsal, *Adv. Mater. Interfaces*, 2015, 185–217.
13 C.-Y. Liu, R. Ram, R. B. Kolaru, A. S. Jana, A. S. Sadhu, C.-S. Chu, Y.-N. Lin, B. N. Pal, S.-H. Chang and S. Biring, *Biosens.*, 2022, **12**, 807.
14 A. Santos, L. Vojkuvka, M. Alba, V. S. Balderrama, J. Ferré-Borrull, J. Pallarès and L. F. Marsal, *Phys. Status Solidi*, 2012, **209**, 2045–2048.
15 T. Kumeria, M. M. Rahman, A. Santos, J. Ferre-Borrull, L. F. Marsal and D. Losic, *Anal. Chem.*, 2014, **86**, 1837–1844.
16 G. Macias, L. P. Hernández-Eguía, J. Ferré-Borrull, J. Pallares and L. F. Marsal, *ACS Appl. Mater. Interfaces*, 2013, **5**, 8093–8098.
17 A. Santos, J. Ferré-Borrull, J. Pallarès and L. Marsal, *Phys. Status Solidi A*, 2011, **208**, 668–674.
18 A. Santos, V. S. Balderrama, M. Alba, P. Formentín, J. Ferré-Borrull, J. Pallarès and L. F. Marsal, *Nanoscale Res. Lett.*, 2012, **7**, 1–4.
19 L. Marsal, L. Vojkuvka, P. Formentin, J. Pallarés and J. Ferré-Borrull, *Opt. Mater.*, 2009, **31**, 860–864.
20 L. Vojkuvka, A. Santos, J. Pallarès, J. Ferré-Borrull, L. Marsal and J.-P. Celis, *Surf. Coat. Technol.*, 2012, **206**, 2115–2124.
21 X. Wang and L. Guo, *Angew. Chem., Int. Ed.*, 2020, **59**, 4231–4239.
22 M. Bechelany, X. Maeder, J. Riesterer, J. Hankache, D. Lerose, S. Christiansen, J. Michler and L. Philippe, *Cryst. Growth Des.*, 2010, **10**, 587–596.
23 A. Kabalnov, *J. Dispersion Sci. Technol.*, 2001, **22**, 1–12.
24 X. Fan, Q. Hao, R. Jin, H. Huang, Z. Luo, X. Yang, Y. Chen, X. Han, M. Sun and Q. Jing, *Sci. Rep.*, 2017, **7**, 2322.
25 T. S. Lednický and A. Bonyár, *ACS Appl. Mater. Interfaces*, 2020, **12**, 4804–4814.
26 A. Arbuz, A. Sultangaziyev, A. Rapikov, Z. Kunushpayeva and R. Bukasov, *Nanoscale Adv.*, 2022, **4**, 268–280.
27 S. Yang, F. Xu, S. Ostendorp, G. Wilde, H. Zhao and Y. Lei, *Adv. Funct. Mater.*, 2011, **21**, 2446–2455.
28 E. Jiran and C. Thompson, *J. Electron. Mater.*, 1990, **19**, 1153–1160.
29 C. Eckstein, L. K. Acosta, L. Pol, E. Xifré-Pérez, J. Pallares, J. Ferré-Borrull and L. F. Marsal, *ACS Appl. Mater. Interfaces*, 2018, **10**, 10571–10579.
30 L. Niu, R. Qin, Y. Liu, J. Xin, X. Wu, F. Zhang, X. Li, C. Shao, X. Li and Y. J. C. I. Liu, *Ceram. Int.*, 2024, **50**, 2611–2622.
31 E. Xifre-Perez, J. Ferre-Borull, J. Pallares and L. F. Marsal, *Open Mater. Sci.*, 2015, **2**, 13–32.
32 X. Fu, T. Jiang, Q. Zhao and H. Yin, *J. Raman Spectrosc.*, 2012, **43**, 1191–1195.
33 C. Muehlethaler, C. R. Considine, V. Menon, W.-C. Lin, Y.-H. Lee and J. R. Lombardi, *ACS Photonics*, 2016, **3**, 1164–1169.
34 X. Liang, B. Liang, Z. Pan, X. Lang, Y. Zhang, G. Wang, P. Yin and L. Guo, *Nanoscale*, 2015, **7**, 20188–20196.
35 Y. Xu, F. Y. Kutsanedzie, M. Hassan, J. Zhu, W. Ahmad, H. Li and Q. Chen, *Food Chem.*, 2020, **315**, 126300.
36 L. Mikac, I. Rigó, L. Himics, A. Tolić, M. Ivanda and M. Veres, *Appl. Surf. Sci.*, 2023, **608**, 155239.

37 F. M. Aldosari, *Molecules*, 2022, **27**, 892.

38 S. He, J. Chua, E. K. M. Tan and J. C. Y. Kah, *RSC Adv.*, 2017, **7**, 16264–16272.

39 Y. Xia and N. J. Halas, *MRS Bull.*, 2005, **30**, 338–348.

40 V. Dhzagan, N. Mazur, O. Kapush, M. Skoryk, Y. Pirko, A. Yemets, V. Dhzahan, P. Shepeliavyi, M. Valakh and V. Yukhymchuk, *ACS Omega*, 2024, **9**, 4819–4830.

41 A. Shiohara, Y. Wang and L. M. Liz-Marzán, *J. Photochem. Photobiol., C*, 2014, **21**, 2–25.

42 X. Fu, T. Jiang, Q. Zhao and H. Yin, *J. Raman Spectrosc.*, 2012, **43**, 1191–1195.

43 J. Yu, M. Shen, S. Liu, F. Li, D. Sun and T. Wang, *Appl. Surf. Sci.*, 2017, **406**, 285–293.

44 C. Muehlethaler, C. R. Considine, V. Menon, W.-C. Lin, Y.-H. Lee and J. R. Lombardi, *ACS Photonics*, 2016, **3**, 1164–1169.

45 J. Liu, J. Zhou, B. Tang, T. Zeng, Y. Li, J. Li, Y. Ye and X. Wang, *Appl. Surf. Sci.*, 2016, **386**, 296–302.

46 Z. Fusco, R. Bo, Y. Wang, N. Motta, H. Chen and A. Tricoli, *J. Mater. Chem. C*, 2019, **7**, 6308–6316.

47 S. Xu, W. Tang, D. B. Chase, D. L. Sparks and J. F. Rabolt, *ACS Appl. Nano Mater.*, 2018, **1**, 1257–1264.